Fifth International Symposium on Marine Propulsors
smp'17, Espoo, Finland, June 2017

Dynamic versus static CFD of Azipod® oblique flow hydrodynamic loads

Mika Nuutinen[1], Pasi Miettinen[1]

[1]ABB Marine & Ports, Helsinki, Finland

ABSTRACT

The oblique flow hydrodynamic loads (forces, moments) of a propulsion unit are required for instance for strength/vibration analysis, component dimensioning and steering force estimations. Perhaps the most straightforward CFD method for this purpose is to conduct simulations at desired number of fixed oblique flow angles. This (static) approach is a simplification of a real (dynamic) situation where the propulsion unit is continually rotated at an angular speed across the range of oblique flow angles. The goal of this research is to conduct dynamic oblique flow CFD simulations of a propulsion unit rotated at realistic angular speed and compare the resulting hydrodynamic loads to corresponding results from static oblique flow CFD simulations. The open water simulations are performed without the ship hull at full scale. Furthermore, advanced modeling methodologies available in CFD software Star-ccm+ (version 10.06.009), such as dynamic fluid body interaction (DFBI) for desired propeller torque and overset meshing for propeller rotation, are utilized. Overall, the loads simulated with static and dynamic approaches are found to behave similarly with dynamic approach predicting higher extreme values. However, the dynamic simulation reveals a massive flow separation from the unit's strut around -35° flow angle, which is not observed in the static simulation. This flow separation produces a strong and sharp peak for instance in the pod unit's moment around main bearing turning axis. The most important finding in this study is that a small number of predetermined static oblique flow angles may not be sufficient for a comprehensive understanding of the loads involved in a realistic situation.

Keywords

Hydrodynamic loads, Dynamic fluid body interaction, Overset mesh.

1 INTRODUCTION

The oblique flow hydrodynamic loads (forces, moments) of a DO-series Azipod unit in oblique flow conditions are simulated at several flow angles in range [-90° ; 90°] (the static approach) and by continuously turning the unit starting from a 0° quasi-steady situation in ranges [0°; 90°] and [0°; -90°] (the dynamic approach). In the static approach, DFBI is utilized by inputting the rotating parts' (propeller blades, hub, electric motor's rotor and axis) moment of inertia and motor torque (set at maximum value). Hence, in the simulations, the propeller rotational speed automatically adapts to fluid loads. Without DFBI, the propeller rotational speed would have to be iterated to attain the desired motor torque. In the dynamic approach, the turning of the unit is preset to accelerate at a constant rate (6°/s^2) until the desired, final turning speed (6°/s) is attained. DFBI for propeller rotation is utilized also in the dynamic approach to maintain the desired motor torque. Finally, the hydrodynamic loads for the unit and its components with these two approaches are compared and elaborated. A wide range of studies regarding oblique flow hydrodynamic loads of podded propulsors has been published. Liu et al(2009) studied podded unit under maneuvering operation with a multibody panel method, Shamsi et al(2014) studied podded drive in azimuthing conditions with CFD, Islam et al(2015) studied podded propulsors in extreme azimuthing conditions with CFD, Xingrong & Yuejin(2013) studied hydrodynamic performance of a podded propulsor at static steering conditions utilizing CFD and measurements, Islam et al(2009) performed measurements of podded propulsor in dynamic azimuthing conditions. This reference list is not exhaustive, and many more studies can be found. It is noteworthy that present authors could not find a single article on modelling the hydrodynamic loads of podded propulsors utilizing the dynamic CFD approach to continually (with realistic acceleration and speed) sweep across the range of oblique flow angles.

2 COMPUTATIONAL DOMAIN, GEOMETRY, MESHING AND BOUNDARY CONDITIONS

2.1 Computational domain

The perimeter of the computational domain is a rectangular box, extending Δx = 140m, Δy = 90m, Δz = 50m (dozens of corresponding pod unit dimensions), centered horizontally at propeller, and top surface located at immersion height above propeller axis.

2.2 Geometry

The simulated pod geometry with part names and their reference coordinate systems (rotated with the pod unit around main bearing CS z-axis in dynamic case), as well as a longitudinal cross section of the computational mesh from static 35° case is shown in Fig. 1. The volumetric

mesh refinement region around the pod is a rectangular box in the static case and a (rotating) cylinder in the dynamic case. In dynamic simulations, the rotation of the pod unit is around the main bearing coordinate system z-axis with clockwise positive rotation angle. In static simulations, the pod unit itself is not rotated but the oblique flow angle is created by inlet velocity direction. Only the streamlining wedge, attached to the "ship bottom", is rotated to align with the inflow direction. The situation in static 35° case is shown in Fig. 2, where the auxiliary coordinate system x-axis corresponds to the direction of travel (the global CS, aligned with the pod unit is shown in the lower left corner for reference). Hence, the inflow velocity is in auxiliary system's negative x-axis direction. The rotating propeller region (modelled as a sliding interface in static simulations) is also highlighted.

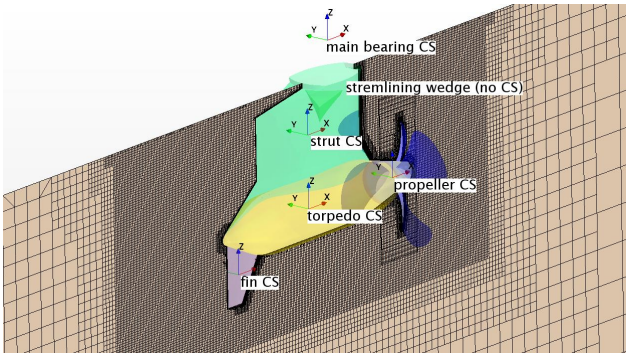

Figure 1: Pod geometry and part names

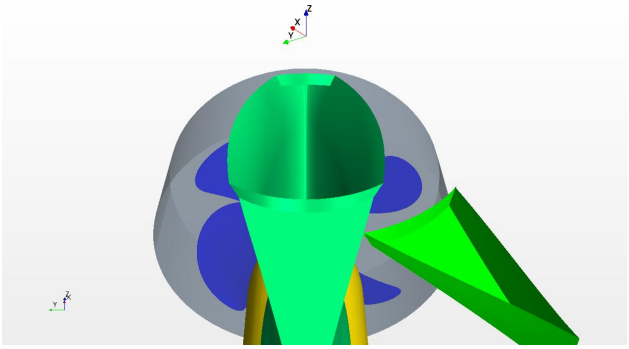

Figure 2: Pod geometry in the static 35° case. Auxiliary CS indicates the direction of travel

Fig. 3 shows the two rotating regions utilized in dynamic simulations. The larger cylinder (modelled as a sliding mesh interface) around the pod unit is for the entire unit rotation and the smaller cylinder (modelled as an overset region for a change) is for propeller rotation. The propeller rotation is set as a superposed motion for the pod unit rotation. The overset method was initially intended also for the pod unit rotation but the refined mesh around the streamlining wedge (in static region) required refined mesh throughout the ring-shaped cut surface on top of the large rotating cylinder. This produced a very large number of computational cells, and it was more practical to utilize sliding interface instead.

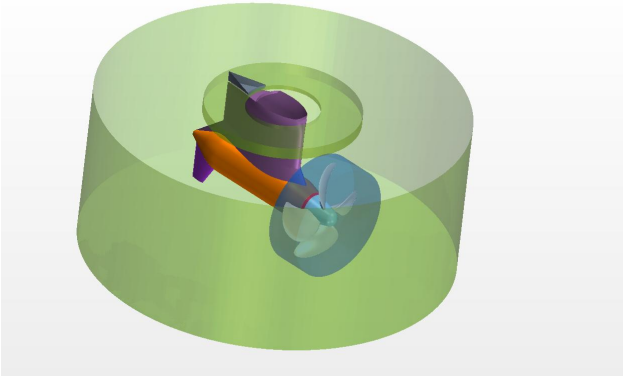

Figure 3: Rotating regions in dynamic simulations

2.3 Meshing

The main meshing parameters are presented in Table 1. The only difference in static and dynamic meshes is the shape of the refinement volume around the pod unit. In static case, the refinement volume is a rectangular box and in dynamic case the refinement volume is the pod unit rotation cylinder.

Table 1. Main meshing parameters

Part(s)	Size target/min	prism layer #/ stretch/thickness
Bounding box	1.667 / 1.667 m	disable
Prop. cylinder	50 / 50 mm	disable
Strut / torpedo / fin / wedge	50 / 5 mm	11 / 1.5 / 69 mm
Vol. control (box or cyl.)	50 mm	-
Prop. blades & hub	25 / 5 mm	11 / 1.5 / 69 mm
Pod unit cyl.	50 / 50 mm	disable

2.4 Boundary conditions

The bounding box x+ and y+/y- planes are set as velocity inlet boundaries, y+/y- depending on the pod angle (see Fig. 2). The x- and y-/y+ planes are set as pressure outlets correspondingly. The top z+ and the bottom z- planes are set as slip walls. All solid boundaries of the pod unit are set as no-slip walls.

3 SIMULATION MODELS

Aside from the DFBI and the overset method, identical numerical models are used for both the static and the dynamic simulations. Simulations are transient with second order spatial and temporal discretizations. A constant timestep is set to correspond to approximately a 2° propeller rotation at max rpm attained at 0° pod angle

and less than 1° propeller rotation at extreme ±90° pod angles (with constant torque, rpm drops with increasing oblique flow angle). The chosen turbulence model is the k-ω-SST with "all y^+ wall treatment". In static simulations, the propeller rotation is controlled by the software's own DFBI model. However, none of the available DFBI options (in Star-ccm+ version 10.06.009) was directly capable of handling the combination of preset pod unit rotation and DFBI controlled propeller rotation, required in the dynamic simulations (it could have been achieved with complicated, nested motions and coordinate systems). Instead, the DFBI propeller rotation was user coded. The governing Euler's equations of motion for combined rotations in principal axis coordinate system are

$$I_x\dot{\omega}_x - \omega_y\omega_z\left(I_y - I_z\right) = M_x \quad (1a)$$

$$I_y\dot{\omega}_y - \omega_z\omega_x\left(I_z - I_x\right) = M_y \quad (1b)$$

$$I_z\dot{\omega}_z - \omega_x\omega_y\left(I_x - I_y\right) = M_z \quad (1c)$$

where I is the principal axis (diagonalized) moment of inertia, ω is the angular velocity (dot above indicates time rate of change) and M is the total moment. Choosing indices x for propeller rotation axis and z for pod unit rotation axis, and setting a constant $\omega_y = 0$ (no tilting motion), Eq. (1a) yields for propeller rotation

$$d\omega_x = \left(M_{x,motor} + M_{x,fluid}\right)/I_x dt \quad (2)$$

which (with $M_{x,fluid}$ from the CFD solution) is integrated for ω_x. The I_x value applied in simulations is an order of magnitude value, not specific to any commercial project. Equations (1b) and (1c) can be seen to produce extra tilting and turning moments in addition to fluid flow induced moments. These extra moments do not affect either of the simulated motions, since ω_y is set to zero and and ω_z is given as a preset motion. These extra moments are easily computed separately and relative values are given in Section 5.3. In Eq. (1b) the moment of inertia components are for the mass rotating with the propeller (blades, hub, propeller axle, and electric motor's rotor), whereas in Eq. (1c), I_z includes the entire pod unit (also the geared turning motors' moment of inertia needs to be fused into this value).

4 SIMULATION PROCEDURES

4.1 Static simulations

In each of the chosen oblique flow angles -90, -50, -35, -15, -5, 0, 5, 15, 35, 50 and 90°, the oblique flow (and inlet/outlet boundary conditions) are set by the inflow direction, the streamlining wedge attached to the "ship bottom" is aligned with the flow, and the geometry is re-meshed. Then the simulation is run until average force/moment values over 10 propeller revolutions can be obtained from quasi-steady time histories. Unless DFBI was utilized, the user would have to monitor the solution and adjust the rpm for target propeller torque (or program a routine to automate this).

4.2 Dynamic simulations

The dynamic simulations (one for negative and one for positive angles) are initialized with a static simulation at 0° (run to quasi-steady state). In both (+/-) simulations, the inflow velocity direction is held constant but the inlet/outlet (y+/y-) boundaries are set so that the propeller always thrusts the fluid towards an outlet and not an inlet boundary. The pod unit rotation has an initial acceleration ramp of ±6°/s^2 until the target rotation rate of ±6°/s is reached, after which the rotation rate is held constant. The simulations are run until the ±90° pod rotation angle is reached, and transient forces and moments, as well as images for animations are recorded. As for comparison with the published research, the work of Islam et al(2009) (experiments on dynamic pod turning), offers the most relevant comparison. However, some central differences should be emphasized. Firstly, the difference in the proportional turning rate (pod turning rate/propeller turning rate) in the present work is roughly twice as large as in the graphical data presented in the reference study. Secondly, the strut (being a "wing" has significant contribution to all loads) is proportionally considerably longer than in the reference study. Thirdly, the propeller rotation in the present study is controlled by a constant torque, allowing the propeller rpm to dynamically adapt to changing load, whereas in the reference study the propeller rpm (advance coefficient) is held constant for a dynamic sweep. This makes direct comparison quite difficult, as the maximum rpm variation in the present study is approximately 50%, see Figure 8. Within range -90°- +90°, the only prominent difference to the reference study is the strong flow separation induced load peak around -30° observed in this study. The root cause is probably a combination of higher relative turning speed and proportionally longer strut in present study. In the present study, strong local peaks are found, but such peaks are difficult to make out from the experimental data presented in the reference study, where stronger variations are found around ±120° (outside the range of the present study).

5 SIMULATION RESULTS

Figures 4 - 7 show snapshot static pressure fields on pod unit surface from static and the dynamic simulations at -35° angle. Although the propeller is at different positions in static/dynamic case figures, the fields look qualitatively very similar. More pronounced differences are observed on the pod unit suction side (Figs. 6 and 7) where the dynamic simulation has more vigorous pressure variations. In the dynamic simulation, there is a massive separation from suction side of the strut just around -30° angle (the surface stalls). This can be seen as the steep collapse in force and moment curves overlaid in Figs. 6 and 7. Figure 8 compares the propeller rotation rates from the dynamic and static simulations. No drastic differences are present, but the dynamic simulation rpms are slightly higher. This is probably due to inertia; in static simulation, the propeller has enough time to reach a quasi-steady state.

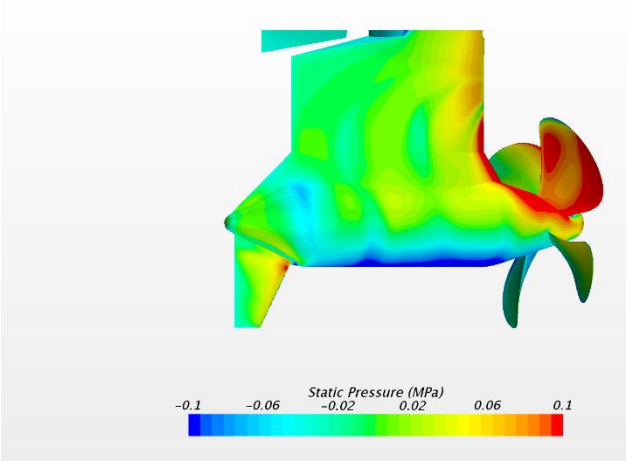

Figure 4: Static pressure on pod unit pressure side surface. Static simulation at -35° angle

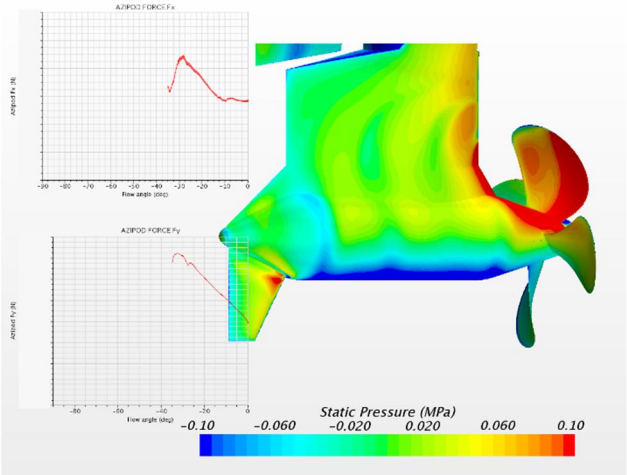

Figure 5: Static pressure on pod unit pressure side surface. Dynamic simulation at -35° angle

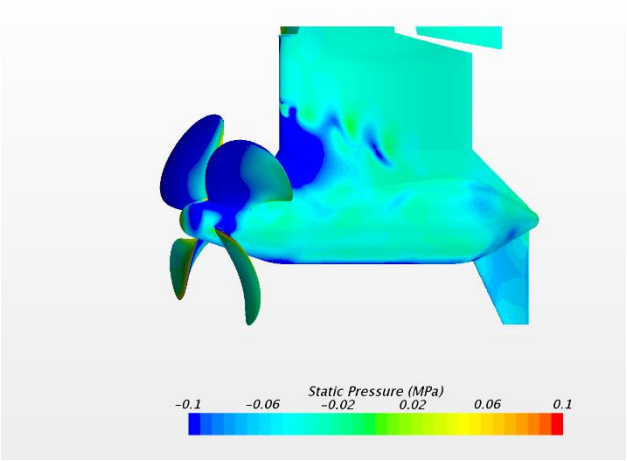

Figure 6: Static pressure on pod unit suction side surface. Static simulation at -35° angle

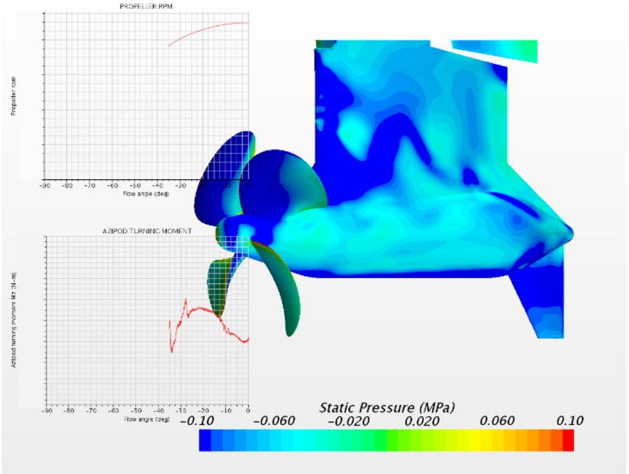

Figure 7: Static pressure on pod unit suction side surface. Dynamic simulation at -35° angle

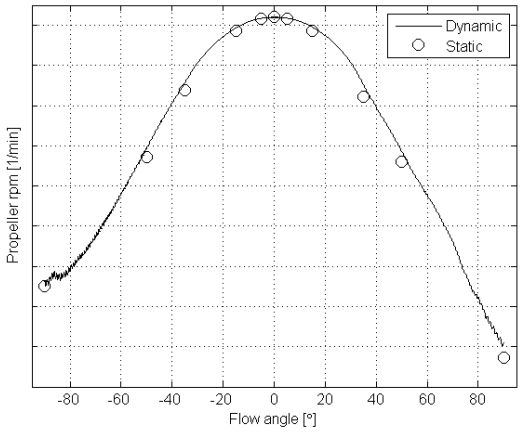

Figure 8: Fixed torque propeller rotation rate

5.1 Hydrodynamic forces

All three force components are recorded for all pod unit parts: the fin, the torpedo, the strut and the propeller. All forces, unless stated otherwise, are given in the main bearing CS, aligned with the pod. Figures 9 - 11 present the forces on the fin. Around -35°, the static simulation misses local F_y and F_z peaks, and towards larger angles the dynamic simulation predicts slightly stronger forces. Otherwise, the dynamic and the static force results for the fin are very similar.

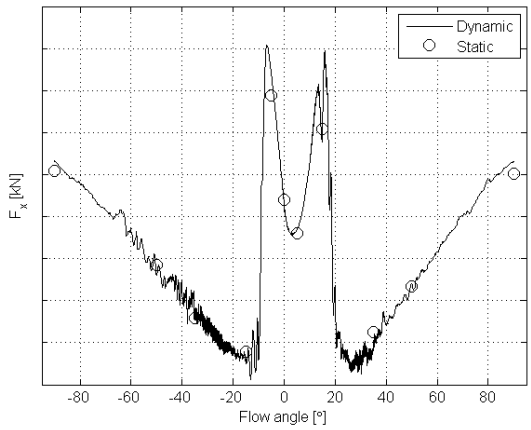

Figure 9: Fin F_x

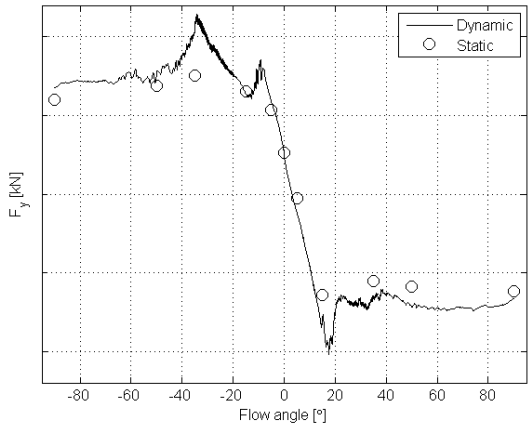

Figure 10: Fin F_y

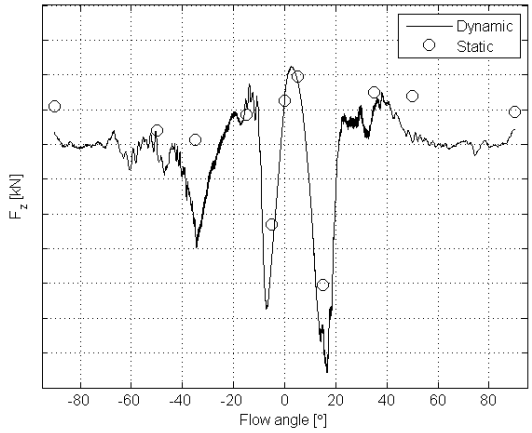

Figure 11: Fin F_z

Figures 12 – 14 present the forces on the propeller. The force levels are very similar throughout (also the force oscillations, although not shown for the averaged static forces).

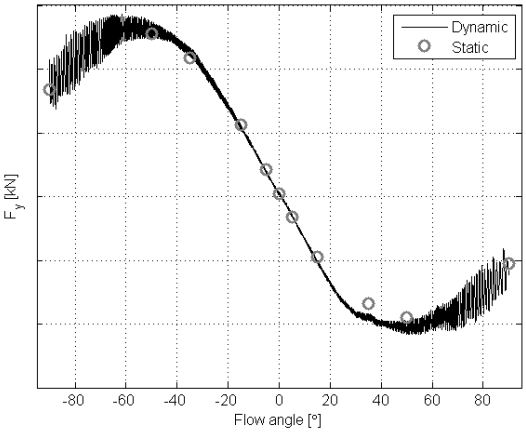

Figure 12: Propeller F_x

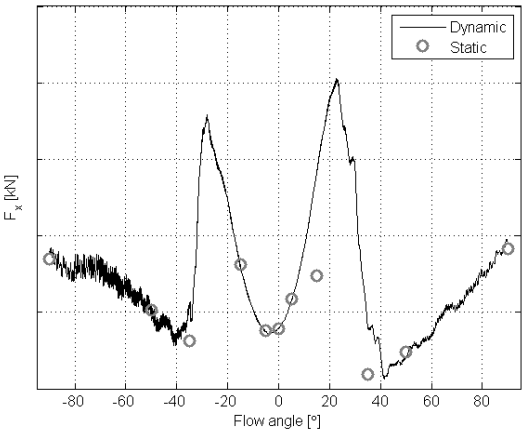

Figure 13: Propeller F_y

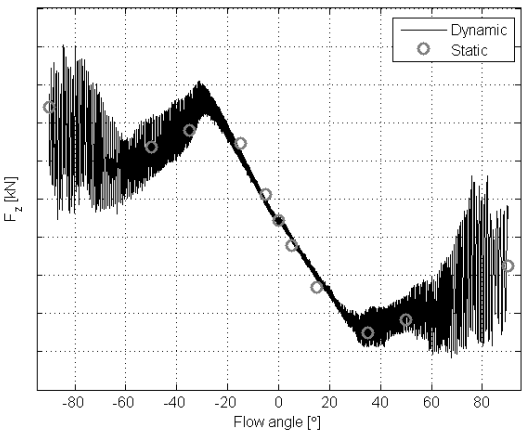

Figure 14: Propeller F_z

Figures 15 – 17 present the forces on the strut. This part exhibits the strongest dynamic effect and underlines the benefit of dynamic simulation: Unless the angles of flow

separation (now around -30° and 20°) are not known a priori, it is likely that the local force extrema are completely missed with static simulations.

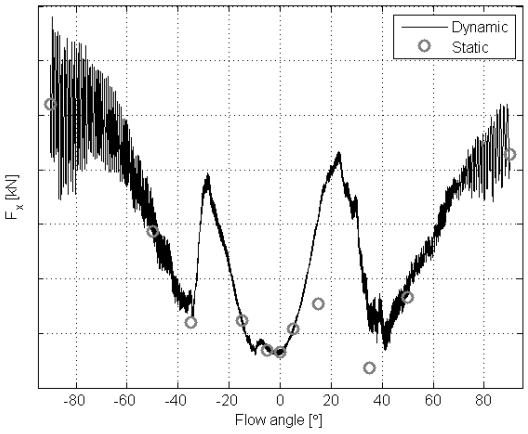

Figure 15: Strut F_x

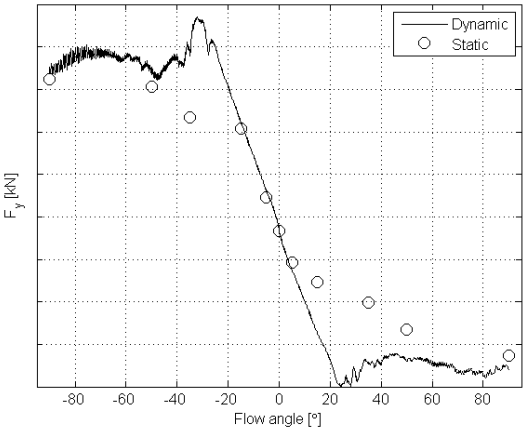

Figure 16: Strut F_y

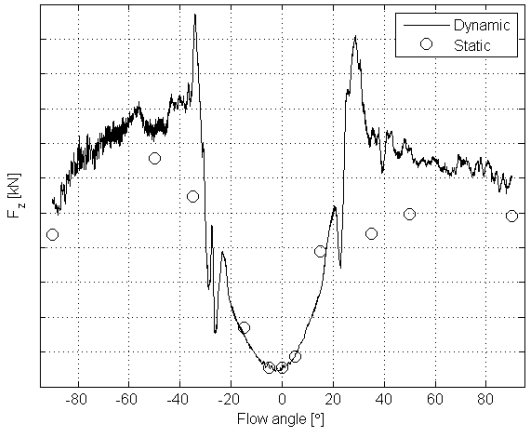

Figure 17: Strut F_z

Figures 18 – 20 present forces on the torpedo. The static/dynamic force levels are similar with largest deviations around ±30°. It is concluded that the strong separation effects on the strut are also reflected on the torpedo forces.

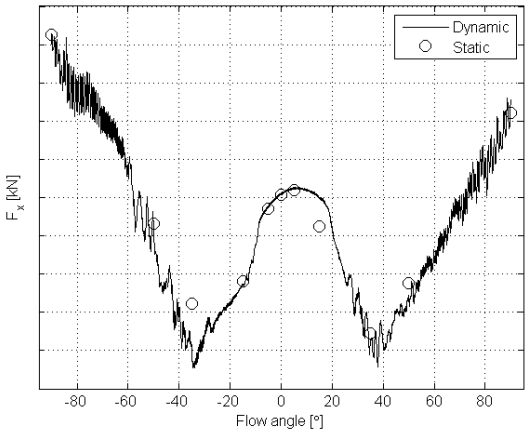

Figure 18: Torpedo F_x

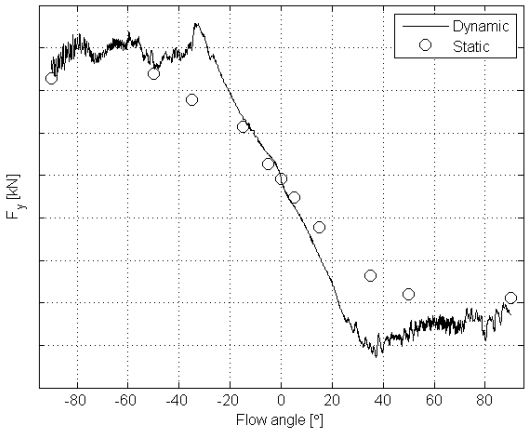

Figure 19: Torpedo F_y

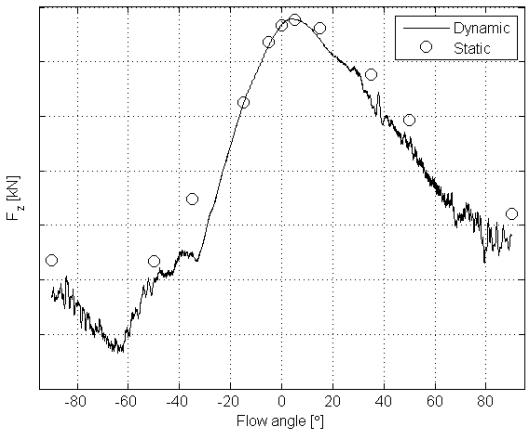

Figure 20: Torpedo F_z

Figures 21 – 23 present the total forces on the pod unit, where the effects shown in Figs. 9 – 20 are combined. It is concluded that the propeller dominates F_x, the strut dominates F_y, and the torpedo dominates F_z. Fig. 24 presents a key dimensioning parameter, the total radial force F_{radial}. Comparing static/dynamic radial/ship CS force values, the differences are again strongest around ±30°.

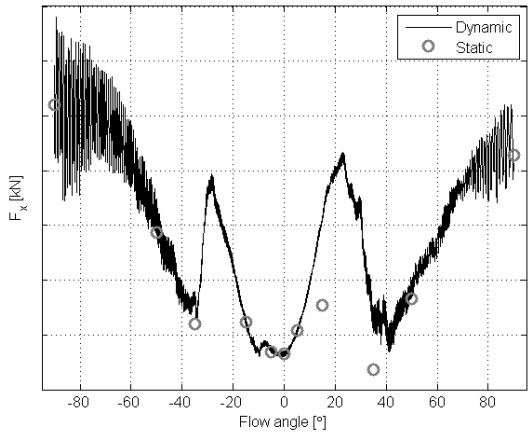

Figure 21: Total F_x

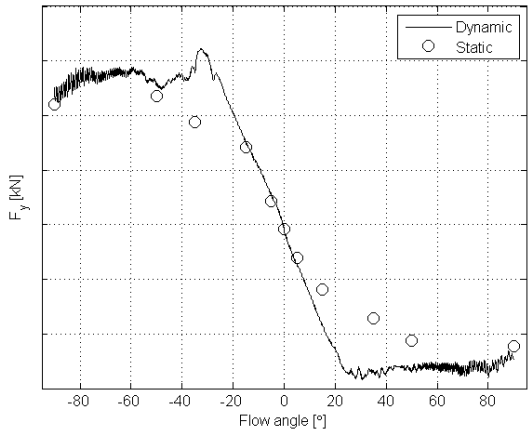

Figure 22: Total F_y

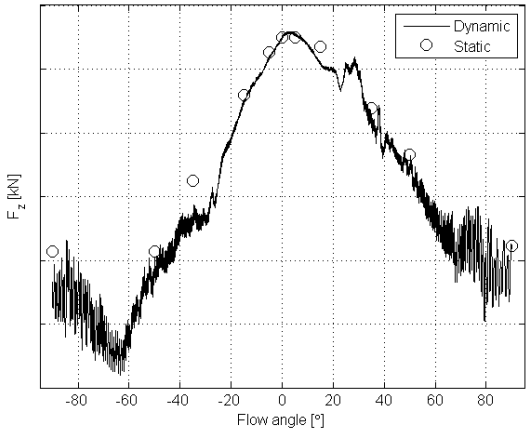

Figure 23: Total F_z

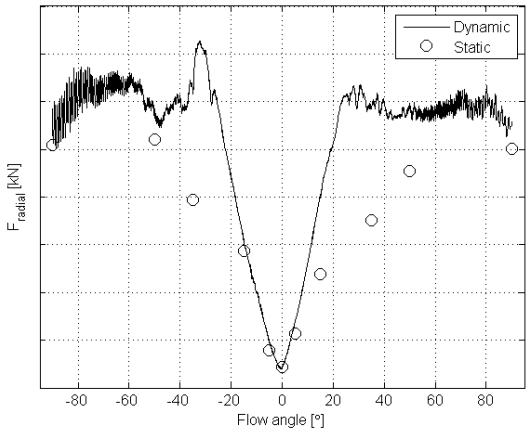

Figure 24: Pod unit radial force

5.2 Hydrodynamic moments

The total hydrodynamic moments around the main bearing CS are presented in Figs. 25 – 27. The static and dynamic moments behave similarly, except around the angles where the flow separates from the strut at -30° and 20°. This finding is important as one criterion for dimensioning the pod unit turning motors is that, for redundancy, a single motor is required to handle ±35° steering angles, and the dimensioning might be underestimated if the strong M_z peak at -35° was missed on grounds of mere static simulation results. The presence and location of these peaks can, of course, be predicted on grounds of prior engineering experience. The number and capacity of the turning motors could then be determined by the overall maximum turning moment and the minimum capacity requirement of a single motor (both with appropriate safety factors). Another key dimensioning parameter, the tilting moment (resultant moment of M_x and M_y) is presented in Fig. 28. This value relates, for instance, to the required robustness of the pod unit's interface to the ship.

Comparing static/dynamic tilting moment values, the differences are again strongest around ±30° angles.

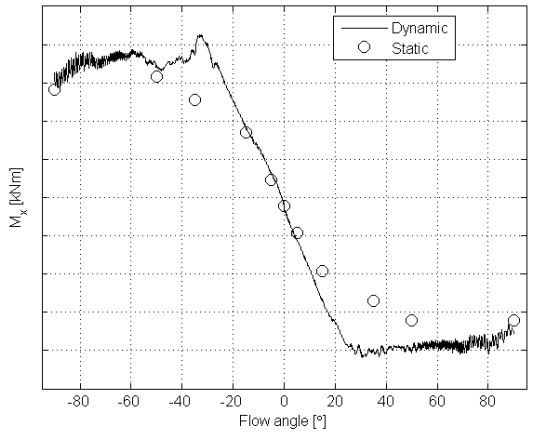

Figure 25: Total moment M_x around main bearing CS

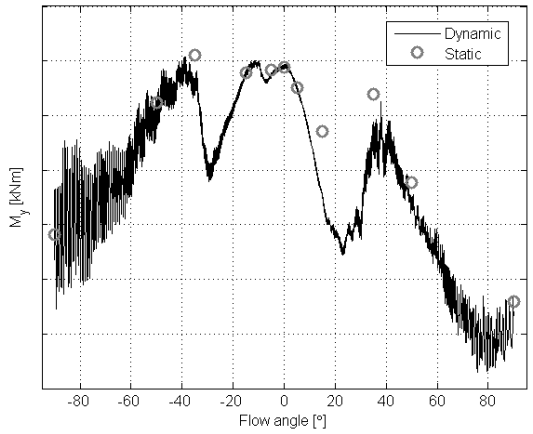

Figure 26: Total moment M_y around main bearing CS

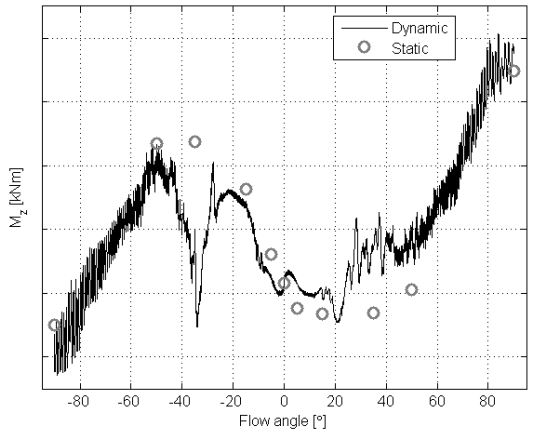

Figure 27: Total moment M_z around main bearing CS

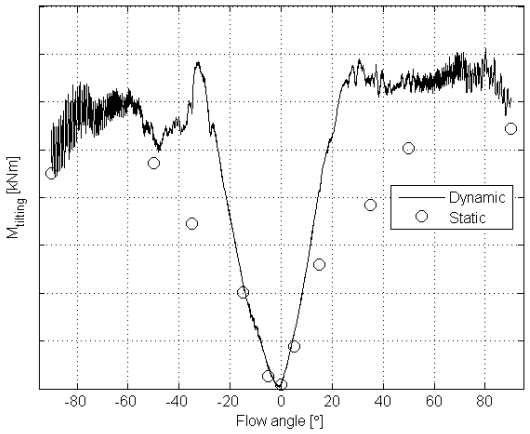

Figure 28: Tilting moment around main bearing CS

5.3 Moments due to inertial effects

As discussed in Section 3, the fluid moment acting on the pod unit is not the total moment transmitted to the main bearing and eventually to the ship hull in dynamic conditions. Using maximum value for propeller rpm and order of magnitude values for the moment of inertia components I_x and I_z (for parts rotating solidly with the propeller), Eq. (1b) yields an extra moment $M_{y,extra}$ whose value becomes around 2% of the corresponding maximum hydrodynamic value. This moment is transmitted from the propeller axis through its bearings to the pod unit and eventually to the ship hull. Again, with order of magnitude value for the moment of inertia component I_z for the entire pod unit (geared turning motors lumped into this value), Eq. (1c) yields an extra moment $M_{z,extra}$ approximately 10% of the corresponding maximum hydrodynamic moment. This is the extra moment the turning motors need to produce in order to accelerate the pod unit rotation at 6°/s^2 around 0° pod angle (in this case this extra moment is required only from 0° to ±3° until the target rotation rate of 6°/s is attained). Should the pod unit rotation be decelerated/accelerated at another angle regime, the resulting extra turning moment would be proportional to the applied rotational acceleration.

6 MESH DEPENDENCE AND SENSITIVITY

In order to verify that the chosen mesh resolution is adequate, the resolution, including the prism layer, near the pod unit (within 0.2 - 0.4 propeller diameters) is doubled in all directions. This refinement approximately doubles the total number of control volumes. The negative angles dynamic simulation is repeated with the refined mesh. The moment M_z around main bearing CS, behaving most vigorously, is chosen for comparison. In Fig. 29, there is a notable, although relatively small phase shift due to the refinement, but overall the original mesh resolution can be deemed sufficient for practical engineering purposes. The

extreme values remain almost equal as does the sudden collapse due to massive flow separation from the strut.

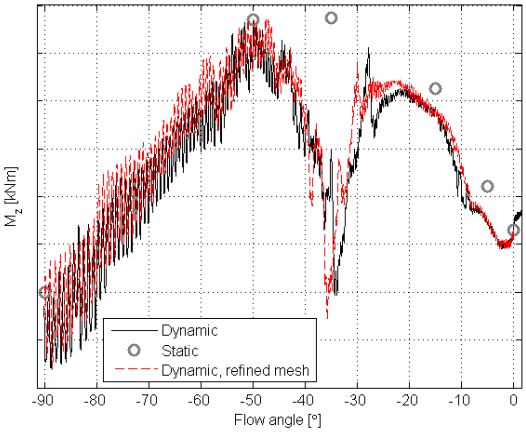

Figure 29: Mesh refinement effect on M_z around main bearing CS

The sensitivity of the solution to the extra sliding interface required for the dynamic pod turning is investigated by running the dynamic simulation (refined mesh) up to -35° (where the discrepancy between static and dynamic results is most prominent) and suddenly stopping the pod turning. Fig. 30 shows (again for main bearing M_z) the effect of separated flow reattaching to the strut and how the moment eventually climbs to oscillate around the corresponding static average (original mesh result). This plot is presented in terms of physical time, t ≈ 7.3s corresponds to -35° (the pod turning starts at t = 1s).

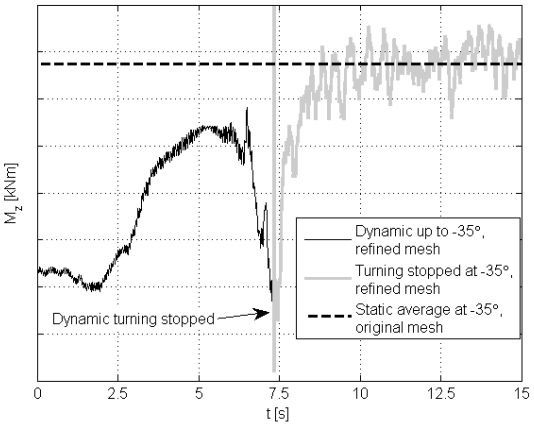

Figure 30: Sensitivity demonstration. M_z around main bearing CS as pod turning is stopped at -35°

7 CONCLUSIONS

Firstly, it is emphasized that all simulation results in this work are produced with a dummy propeller geometry and order of magnitude values for moments of inertia. Thus, the results are not representative of any real commercial project. Only comparative assessment between the static and the dynamic approaches is feasible.

The most important finding in this study is that a small number of predetermined static oblique flow angles may not be sufficient for a comprehensive understanding of the loads involved in a realistic situation. In present, exemplary study, the massive flow separation from the strut suction side is completely missed with the static simulations, and the overall levels of central dimensioning parameters like the pod unit radial force, turning moment and tilting moment are underestimated with the static approach. Hence, the dynamic approach is a strongly recommended aid for engineers in dimensioning purposes. The dynamic approach is computationally faster than the static approach, since there is no need to simulate each angle to quasi-steady state. Furthermore, it is a relatively simple task to simulate different kinds of situations with the dynamic approach. For instance, crash stop, any kind of maneuvering routine or a sudden loss of propulsion/turning motor power.

REFERENCES

Islam, M., Jahra, F., Ryan, R., and Hedd, L. (2015). 'Hydrodynamics of Podded Propulsors With Highly Loaded Propellers and in Extreme Azimuthing Conditions'. ASME 2015 34th International Conference on Ocean, Offshore and Arctic Engineering, Volume 11: Prof. Robert F. Beck Honoring Symposium on Marine Hydrodynamics St. John's, Newfoundland, Canada, May 31–June 5, 2015.

Islam, M., Akinturk, A., and Veitch, B., Liu, P. (2009). 'Performance Characteristics of Static and Dynamic Azimuthing Podded Propulsor. First International Symposium on Marine Propulsors smp'09, Trondheim, Norway, June 2009.

Liu, P., Islam, M., Veitch, B. (2009). 'Unsteady hydromechanics of a steering podded propeller unit'. Ocean Engineering **36** (12-13), pp.1003-1014.

Shamsi, R., Ghassemi, H., Molyneux, D., and Liu, P. (2014). 'Numerical hydrodynamic evaluation of propeller (with hub taper) and podded drive in azimuthing conditions'. Ocean Engineering **76** (15), pp.121-135.

Xingrong, S., and Yuejin, C. (2013). 'Study on Hydrodynamic Performance of Podded Propulsor at Steering Conditions'. Third International Symposium on Marine Propulsors smp'13, Launceston, Tasmania, Australia, May 2013.